Self-Assembly of Nanoparticles into Rings: A Lattice-Gas Model

Guy Yosef and Eran Rabani*

School of Chemistry, The Sackler Faculty of Exact Sciences, Tel Aviv University, Tel Aviv 69978, Israel

Received: June 13, 2006; In Final Form: July 30, 2006

A coarse-grained lattice-gas model in three dimensions is developed to study the self-assembly of nanoparticles into micrometer-sized rings from a thin liquid film containing the nanoparticles. The model describes the nanoparticles as well as the solvent on length scales that are typical of the solvent bulk correlation length. Morphologies obtained from simulations of the model resemble recent experiments and provide a microscopic picture for the formation of nanoparticle rings. The role of evaporation rate, film thickness, diffusion rate, and nanoparticle coverage is discussed and compared to other continuum theories. Predictions of novel structures resulting from low nanoparticle mobility are analyzed.

Introduction

In recent years, there has been growing interest in the fabrication of structures on the nanometer scale.[1] Most of the effort has been devoted to the fabrication of novel nanomaterials[2−7] and the assembly of these building blocks into well-defined ordered arrays.[8−17] Although exquisite control over the composition, size, shape, and surface properties of materials on the nanometer scale can now be achieved, control over their assembly into predefined superstructures is still quite limited.

The fabrication of nanomaterials and their assembly into superstructures share many common features. For example, both processes are out-of-equilibrium and are kinetically driven. However, there are significant differences that limit the control of the assembly into predefined ordered superstructures. First, the energy scales are different: The synthesis of nanomaterials is driven by chemical forces much stronger than the physical forces that drive the assembly process. Furthermore, despite the fact that both processes are carried out in solutions, only the assembly process is triggered by the evaporation of the solvent.

Often, various self-assembled phases form when a liquid containing nanoparticles evaporates.[18−21] The formation of these morphologies is governed by a subtle interplay of a variety of influences. One of the key factors that govern the precipitation and self-assembly processes involves various interactions between nanoparticles, substrates, and solvents.[22−26] Other factors include the drying kinetics,[27−32] hydrodynamic effects,[33−35] and the self-diffusion of the nanocrystals on the substrate.[36]

Recently, several groups have observed the formation of large rings made of nanoparticles.[33−35,37−42] A typical AFM image of such a ring is shown in Figure 1. Ohara and Gelbart[43] have developed a theoretical model to explain the assembly of nanoparticles into ring-shaped structures. They argued that micrometer-sized rings were formed from holes nucleating in volatile, wetting thin liquid films containing the nanoparticles.[43] The nucleation of holes in this thin film can occur because of evaporation or disjoining pressure.[44] Each ring formed from the pinning of the rim of an opening hole by a sufficient number of particles.

In the present study, we develop an approach complimentary to that presented by Ohara and Gelbart. We focus on the case where the driving force for hole nucleation and growth is due to evaporation. Our approach is based on a coarse-grained model and includes the description of the nanoparticles as well as that of the liquid on length scales that are equal or larger than the typical correlation length of bulk liquid. Small length scale fluctuations, which are typically Gaussian, will be integrated out.[45]

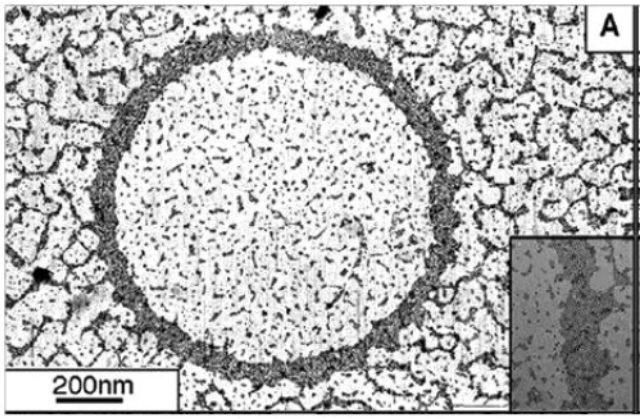

Figure 1. Silver nanocrystals deposited on a TEM grid. Picture courtesy of Marie-Paule Pileni from ref 34.

Our approach is different from that developed by Ohara and Gelbart in several ways. First, the solvent fluctuations are described on length scales typical of the size of the nanoparticles, whereas Ohara and Gelbart used a continuum approach and described fluctuations of the solvent on length scales comparable to the size of the rim. Thus, our approach provides a microscopic description of the structure and the mechanism of the formation of rings. Furthermore, because the nanoparticles are treated explicitly and their motion is described microscopically, our approach can be used to study the interplay between the dynamics of hole formation and growth and the diffusion of the nanoparticles. Last, the evaporation conditions are determined solely by the chemical potential and the temperature, whereas the model of Ohara and Gelbart is phenomenological and is based on several assumptions made for the rates of evaporation, hole growth, and fluid flow.

We find that most qualitative features predicted by Ohara and Gelbart are well-described by our coarse-grained model.

* To whom correspondence should be addressed. E-mail: rabani@tau.ac.il.

10.1021/jp063668u CCC: $33.50
Published on Web 10/05/2006

However, several quantitative features emerging from our theory are quite different in comparison to the theory of Ohara and Gelbart.

The outline of our paper is as follows. In Section II, we present the coarse-grained lattice-gas model and other simulation details. We develop a model in three dimensions appropriate for a thin liquid film containing the nanoparticles. Our model also includes an explicit description of the substrate. In Section III, we present simulation results of our model for different model parameters. We study the role of nanoparticle diffusion, concentration, film thickness, and evaporation conditions on the resulting shape, size, and width of the rings. We also discuss the importance of simulations in three dimensions compared to the two-dimensional case. Finally, in Section IV, we conclude.

II. Model

In this section, we develop a lattice gas model to describe the drying-mediated self-assembly of nanoparticles into rings. Furthermore, we specify the Monte Carlo procedure we applied to study the lattice-gas dynamics and other simulation details.

A. Lattice-Gas Model. The coarse-grained lattice gas model we developed to describe the self-assembly of nanoparticles into a ring-shaped structure is an extension of the model developed by Rabani et al. for the 2D system[29] and is similar to that presented by Sztrum et al. for the 3D case.[30] The solvent and nanoparticles in our model are represented as a three-dimensional lattice gas.[46] Each cell of a cube lattice can be occupied by either liquid or nanoparticle or vapor. The substrate (surface) is also modeled by a lattice gas. The size of each cell in the lattice equals the typical solvent correlation length, $\xi \sim 1$ nm. Because the size of a nanoparticle can exceed the range of correlated solvent fluctuations, we allow them to span several cells of the lattice (the results reported below were carried out for nanoparticles with lattice cells of size $2 \times 2 \times 2$). The lattice-gas Hamiltonian can be expressed in terms of three binary variables, l_i, n_i, and s_i

$$H = -\sum_{\{ij\}} \epsilon_l^{i-j} l_i l_j - \sum_{\{ij\}} \epsilon_n^{i-j} n_i n_j - \sum_{\{ij\}} \epsilon_{nl}^{i-j} n_i l_j - \epsilon_{\mathrm{ns}} \sum_{<ij>} n_i n_j - \epsilon_{\mathrm{ls}} \sum_{<ij>} l_i s_j - \mu \sum_i l_i \quad (1)$$

where l_i, n_i, and s_i are roughly proportional to the density of the solvent, nanoparticles, and substrate at lattice site i, respectively.[45] Each binary variable can equal to 0 (low density) or 1 (high density). A single lattice site cannot be occupied by more than one species to incorporate excluded volume effects.

Our model is different from that used by Sztrum et al.[30] in that not only nearest but also next-nearest neighbors are taken into account when calculating the energy change associated with the nanoparticles and the solvent. As pointed out by Martin et al.,[32] this modification is necessary to compensate for anisotropy observed in the heterogeneous limit of evaporation. Thus, the first three terms on the right-hand side of eq 1 include both first- and second-nearest neighbors (indicated by the sum $\sum_{\{ij\}}$), whereas the next terms on the right-hand side of eq 1 representing the interactions with the substrate include only first-nearest neighbors (indicated by the sum $\sum_{<ij>}$). In the 3D model presented above, there are six nearest-neighbor lattice cells and 12 second-nearest-neighbor lattice cells.

The different cells attract one another with a strength that depends on the occupation of the two cells and the distance between these cells. The strength of the interactions between adjacent, first-nearest-neighbor cells occupied by the liquid is given by ϵ_l, whereas the next-nearest-neighbor interaction is scaled and is given by[32] $(1/\sqrt{2})\epsilon_l$. Similarly, when two cells are occupied by nanoparticles, they attract one another with a strength given by ϵ_{n} and $(1/\sqrt{2})\epsilon_{\mathrm{n}}$, for first-nearest neighbors and second-nearest neighbors, respectively.

Adjacent cells that are occupied by different species also attract one another. The strength of nanoparticle−liquid attractions is given by ϵ_{nl} and $(1/\sqrt{2})\epsilon_{\mathrm{nl}}$ for first-nearest neighbors and second-nearest neighbors, respectively. Only first-nearest neighbors are included for the attractions of the nanoparticle and the solvent with the substrate. These are given by ϵ_{ns} and ϵ_{ls} for the nanoparticle−substrate and liquid−substrate attractions, respectively. Note that we exclude the constant term $\epsilon_s \sum_{<ij>} s_i s_j$ from the Hamiltonian, because the value of the substrate binary variables is fixed in the simulations reported below.

To prevent aggregation of nanoparticles in the presence of the liquid,[11] we take $\epsilon_l < \epsilon_{\mathrm{nl}}$. In addition, the attraction between the nanoparticles is taken to be larger than the attraction between the nanoparticles and the liquid, i.e., $\epsilon_{\mathrm{nl}} < \epsilon_{\mathrm{n}}$, so that the nanoparticles tend to aggregate in the absence of liquid.[22−26] This constraint is also consistent with the highly polarizable nature of the nanoparticle core.[47,48] More specifically, we set $\epsilon_{\mathrm{n}} = 2\epsilon_l$ and $\epsilon_{\mathrm{nl}} = (3/2)\epsilon_l$ in all the results reported below. The attractions between the solvent and the substrate and between the nanoparticles and the substrate are taken to be $\epsilon_{ls} = (1 + 2\sqrt{2})\epsilon_l$ and $\epsilon_{\mathrm{ns}} = (1 + 2\sqrt{2})\epsilon_{\mathrm{n}}$, respectively. This set of parameters ensures that the liquid wets the substrate ($\epsilon_{ls} \geq (1 + 2\sqrt{2})\epsilon_l$) and that the attractions between the nanoparticles and the liquid are similar in magnitude to the attractions between the nanoparticles and the substrate (given that the latter include only first-nearest neighbors), so that the nanoparticles are not driven to the substrate when it is wet. We note in passing that the conclusions drawn from our work are not affected when we vary these parameters within a reasonable physical range.

The last term on the right-hand side of eq 1 describes the chemical potential, μ, that is used to establish the average concentration of liquid and vapor cells at equilibrium. A large negative value of μ will favor evaporation, whereas positive values will favor wetting. The crossover from wetting to evaporation occurs at $\mu = -3(1 + \sqrt{2})\epsilon_l$. Because the vapor pressure of the nanoparticles and the substrate is negligibly small, we do not include a chemical potential for these species in the Hamiltonian. In other words, the binary variables associated with the nanoparticles and the substrate (n_i and s_i, respectively) conserve the corresponding densities (conserved order parameter), whereas the binary variable representing the liquid does not conserve density (nonconserved order parameter).[49]

The number of cells in each dimension is given by h_α with $\alpha = x, y, z$. An experimental realization of a thin film of nanoparticles deposited on a substrate is described by large values of h_x and h_y, typically several hundreds to thousands of cells representing a layer several micrometers square in area. The z direction describes the height of the wetting layer. In the results reported below, we used $h_x = h_y = 1500-2400$, and h_z varies between 4 and 32 cells, corresponding to a solvent film of several to several tens of nanometers. We assume periodic boundary conditions in the $x-y$ plane only.

B. Monte Carlo Dynamics. The dynamics of our model are stochastic, both for solvent density fluctuations and for nanoparticle diffusion. In the former case, configurations evolve by Monte Carlo dynamics. We attempt to convert a randomly chosen lattice cell i, one that is not occupied by a nanoparticle

or the substrate, from liquid to vapor (or vice versa), $l_i \rightarrow (1 - l_i)$. In the case that $l_i = 1$, we attempt such a move only if the first-nearest-neighbor lattice cells are not completely occupied by the liquid or the nanoparticles or the substrate. In the case that $l_i = 0$, we attempt such a move only if at least one first-nearest-neighbor lattice cell is occupied by the liquid or the nanoparticles or the substrate. These moves are then accepted with a Metropolis probability, $p_{acc} = \min[1, \exp(-\Delta H/k_B T)]$, where k_B is the Boltzmann constant and ΔH is the resulting change in energy computed using the Hamiltonian given by eq 1. The main motivation to use this set of constraints on the liquid moves is to avoid unphysical situations in which nanoparticles are surrounded by vapor (away from the substrate) in the limit of rapid evaporation. In this move, the dynamics do not conserve solvent density within the film, as seems appropriate for an evaporating thin film solution.

As mentioned before, the nanoparticles have negligible vapor pressure, and therefore, their density should be conserved. Thus, in our model, they execute a random walk on the three-dimensional lattice, biased by their interactions with each other, with the liquid cells, and with the substrate. Hence, the diffusion rate of the nanoparticles is affected by the interactions between the nanoparticles where the energetics associated with this are the nanoparticle−nanoparticle surface tension. However, our model neglects frictional forces arising from the interactions with the substrate.

In detail, we attempt to displace a nanoparticle by a single lattice spacing in a randomly chosen direction. Such a move is accepted with the same Metropolis probability, but only if the region into which the nanoparticle moves is completely filled with liquid. Solvent density in lattice cells overtaken by this displacement is regenerated in the wake of the moving nanoparticle. This final constraint mimics the very low mobility of nanocrystals on a dry surface.[36] It also provides an additional coupling between the kinetics of evaporation and nanoparticle phase separation.[29,30]

In all the results reported below, a single Monte Carlo step consists of an attempt to change the value of all liquid/vapor cells (note that the sum of liquid and vapor cells is conserved) followed by N_{move} attempts to move all nanoparticles. Thus, the diffusion rate of the nanoparticles is controlled by changing the value of N_{move}.

C. Initial Conditions. All simulations reported below start from a nonequilibrium initial condition in which the 3D lattice is entirely filled with liquid and nanoparticles, except for the lowest layer, which is filled with the substrate (the value of the lattice cells in the lowest layer, representing the substrate, is fixed for the entire simulation), and a hole (cylinder of radius R (R will also be used to designate the radius of the ring) and length h_z) placed at the center of simulation box, which is filled with gas (void). The diameter of the cylinder is taken to be several tens of lattice sites. The results are independent of the size of this hole as long as the conditions are such that the hole grows with time.

The nanoparticles acquire random position inside the simulation box (excluding the volume of the hole and the volume of the substrate) at a given coverage or molar ratio. We fix μ at a value for which the equilibrium state is vapor (i.e., $\mu < -3(1 + \sqrt{2})\epsilon_l$) and follow the dynamics of nanoparticle assembly coupled to the dynamics of the solvent evaporation.

These initial conditions seem appropriate for experiments of a thin liquid film containing nanoparticles that completely wet the substrate, where because of evaporation or disjoining pressure, a small hole opens up.[43] We focus on the stage of hole growth, which is effectively separated from the rare event of hole nucleation in thin liquid films.[43]

III. Results and Discussions

In Figure 2, we plot snapshots of the 3D simulated trajectory at different times at a thermodynamic state corresponding to a nanoparticle coverage $\rho = 0.09$, chemical potential $\mu = -7.625\epsilon_l$, and temperature $T = (1/2)\epsilon_l$. Only the positions of the nanoparticles at the even lowest eight layers are shown (here, $h_z = 16$). The values of μ and T correspond to a total evaporation time of $\tau_l \approx 400$. This evaporation time corresponds to the time at which the initial liquid density is reduced to $\approx 1/3$. The value of $N_{move} = 80$ corresponds to nanoparticle motion time of $\tau_n = \xi^2/D_{xy} \approx 0.075$ in units of Monte Carlo steps (MCS), so that $\tau_l/\tau_n \approx 5333$. Here, D_{xy} is the 2D nanoparticle diffusion coefficient in solution and ξ is the typical size of a lattice cell (see Section II). Under these conditions, we find that the uniform and rim evaporation rates are nearly constants[43] over the entire period of simulation, with $dR/dt \approx 1$ and $dh_z/dt \approx 0.05$ in MCS. This implies that the growth of the ring is approximately 20 times faster than the change in the film thickness. In fact, we find that rings can be formed only when $dR/dt \gg dh_z/dt$.

At early times, nanoparticles fill random cells in the simulation box. The remaining cells are filled with liquid, excluding the cylindrically shaped hole at the center of the simulation box. The evolution of the this nonequilibrium initial condition is driven by the value of the chemical potential, which favors evaporation and subsequently results in the growth of the vapor hole. Evaporation occurs layer-by-layer, and solvation forces drive the nanoparticles in the direction of the substrate, until a thin wet layer of disordered nanoparticles is formed. During this time, the vapor hole continues to grow and solvation forces also drive the nanoparticles away from the growing hole, where they begin to accumulate along the rim. Eventually, long wavelength fluctuations of the liquid density lead to a sudden evaporation of the thin liquid layer. Following this evaporation, domain edges become effectively frozen so that aggregation essentially halts. The nanoparticles freeze along the rim to form the micrometer-size ring, as shown in the last time frame of Figure 2. The similarity between the last frame shown and the experimental TEM image shown in Figure 1 is remarkable.

The formation of the ring structure has been described, so far, by a lattice-gas model in 3D. As can be seen in Figure 2, the final morphology is flat and the resulting ring can effectively be described in 2D. This raises an interesting theoretical question of whether the formation of rings can be described by a lattice-gas model in 2D rather than the one we proposed in 3D. To answer this question, we have carried out simulations under similar conditions using a 2D model described elsewhere[29] with initial conditions that also include a small circular hole at the center of the simulation box. So far, all attempts to form stable rings using the reduced 2D model failed.

There are several differences in the evaporation dynamics and hole growth when comparing results obtained from the 2D and 3D models. In the 3D model, evaporation at the rim leads to hole growth and at the same time, evaporation reduces the height of the film but does not open other holes. Only when the thickness of the liquid film is small, on the order of a monolayer, do other holes open up. At this stage, when the evaporation of the thin layer is fast, the liquid disappears uniformly, and the nanoparticle freeze at the rim with traces of small islands outsize the ring. This is not the case for the 2D model, where in addition to the hole growth, other holes open up and grow at nearly the same pace. This leads to morphologies

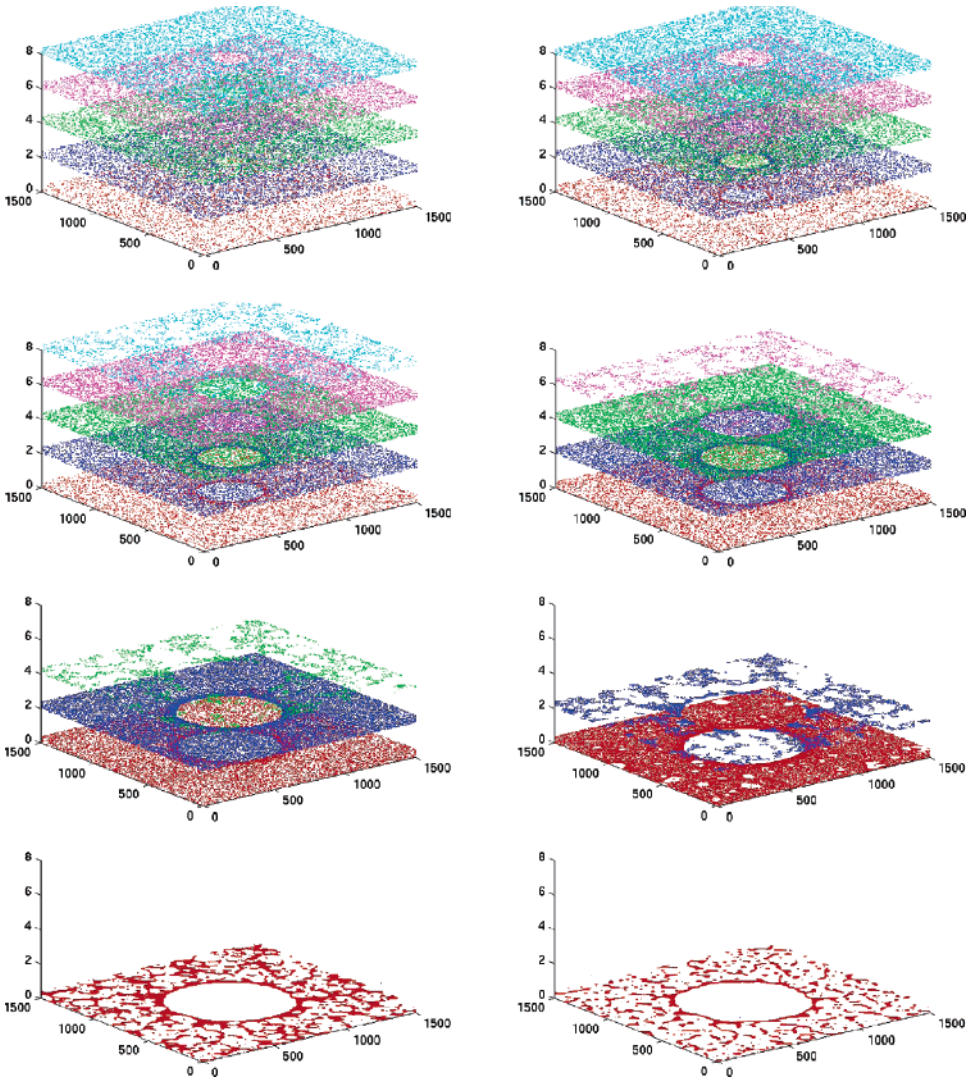

Figure 2. Snapshots of simulated trajectories at different times. From top left to bottom right: $t = (1/4)\tau_l$ to $t = 2\tau_l$ in steps of $(1/4)\tau_l$, where $\tau_l \approx 400$ is the evaporation time in Monte Carlo steps. The nanoparticle coverage, chemical potential, temperature, and nanoparticle motion are $\rho = 0.09$, $\mu = -7.625\epsilon_l$, $T = (1/2)\epsilon_l$, and $N_{\mathrm{move}} = 80$, respectively. Different colors represent the position of nanoparticle at different layers (only the lowest 8 layers are shown in steps of two layers).

that are typical of those observed under heterogeneous evaporation dynamics in the 2D model.[29] Namely, the locations of nanoparticle domains at long times roughly trace the intersection lines of colliding vapor holes, leading to networklike morphologies. Thus, the formation of rings requires separate control over (a) the rate of evaporation, (b) the rate of hole growth, and (c) the rate of hole nucleation. These are controllable in the 3D model but not in the 2D reduced version.

The mechanism described above for the formation of rings is slightly different from that proposed before.[43] As the vapor hole continues to grow, the density of nanoparticles accumulates along the rim. However, because the solvation forces are strong and the nanoparticles are quite mobile (despite the fact that their mobility decreases when their density increases), the higher density of nanoparticles along the rim does not lead to arrest. Rather, it is the evaporation of the final liquid layer that freezes the system and stops the growth process.

To better understand the mechanism proposed above and to delineate the parameters that control the size and shape of the ring, we have carried out simulations at different model parameters. Variations were carried out for the nanoparticle density, evaporation rate, film thickness, and nanoparticle diffusivity.

In Figure 3, we show snapshots from simulated trajectories of the formation of rings for different nanoparticle densities (2D density), ranging from $\rho = 0.06$ to $\rho = 0.19$. We fix the values of the chemical potential and nanoparticle mobility to $\mu = -8\epsilon_l$ and $N_{\mathrm{move}} = 100$, respectively. We observe that the diameter of the ring hardly changes as the nanoparticle density is increased within the range of densities studied. This supports the mechanism proposed above, where the correlation between the hole growth and the density of nanoparticles at the rim is small and does not affect the growth process itself. It is in contrast to the mechanism proposed by Ohara and Gelbart, in which more concentrated solutions particles accumulate more rapidly along the rim of the opening holes, leading to earlier pinning and hence smaller rings.[43] This discrepancy can result from the narrow range of densities studied in this work or from the fact that we neglect the friction force between the nanoparticles and the substrate. However, we believe that it is an inherent property of the proposed mechanism of pinning, which is different from that proposed in ref 43 (for further discussion, see the Conclusions).

The major effect of changing the density of nanoparticles is depicted in Figure 4, where we plot the radial density of nanoparticles averaged over 15 trajectories for the same model

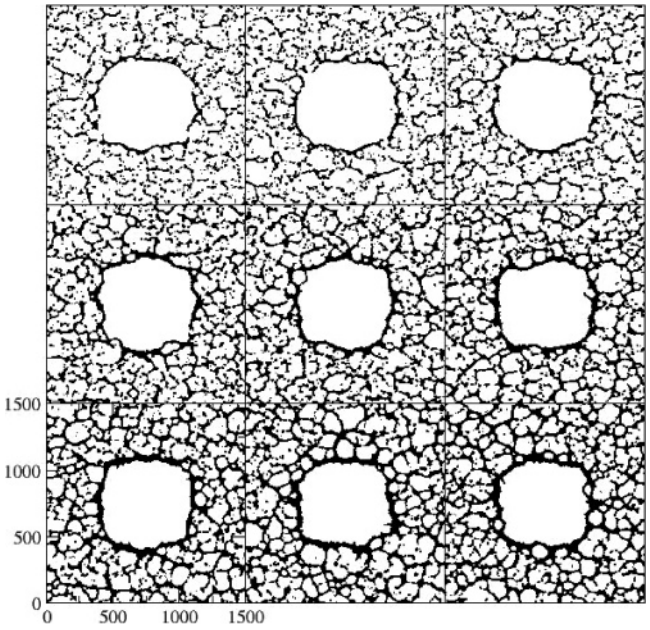

Figure 3. Final morphologies of ring formation for different nanoparticle coverage. Only the lowest layer is shown. The chemical potential, temperature, and nanoparticle motion are $\mu = -8\epsilon_l$, $T = (1/2)\epsilon_l$, and $N_{move} = 100$, respectively. Nanoparticle coverage (from top left to bottom right): 0.06, 0.07, 0.08, 0.12, 0.13, 0.14, 0.17, 0.18, and 0.19, respectively.

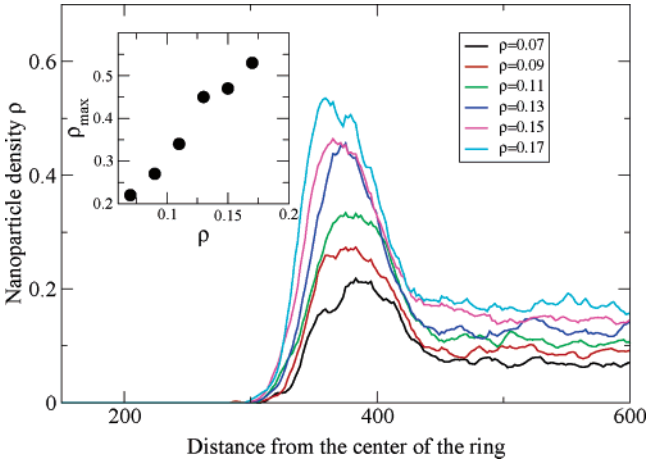

Figure 4. Plots of the radial density of nanoparticles for different nanoparticle coverage averaged over 15 different MC runs. Model parameters are identical to those in Figure 3. Inset shows the maximum value of nanoparticle density as a function of their coverage.

parameters used in Figure 3. The profile of all curves is very similar, and the value at which the density profile approaches its maximal value is nearly independent of the nanoparticle density. The density of nanoparticles inside the ring is negligibly small. As the distance approaches the radius of the ring, the density of nanoparticles increases to a maximal value. At large distances away from the center of the ring, the density of nanoparticles approaches a constant value that equals the coverage corresponding to that specific density of nanoparticle. The maximum value of the density correlates linearly with the coverage of nanoparticles, as can be seen in the inset shown in Figure 4.

The effects of changing the height of the thin liquid layer and the rate of evaporation by changing the chemical potential are shown in Figure 5. The nanoparticle coverage is $\rho = 0.1$, the temperature is $T = (1/2)\epsilon_l$, $N_{move} = 80$, and the chemical potential is $\mu = -8\epsilon_l$. As predicted by Ohara and Gelbart, the change in the height of the film has a significant effect on the hole diameter.[43] We find that in the limit where evaporation is dominant, the diameter of the ring scales linearly with the film thickness. This is consistent with the picture that evaporation occurs layer by layer, and thus, an increase in the film thickness results in an increase in the time window for ring growth.

A more dramatic effect on the ring diameter is observed when the chemical potential is varied, as shown in the right panel of Figure 5. The model parameters are the same as for the left panel of Figure 5, but for a fixed film thickness of $h_z = 16$. In our model, the chemical potential is used to control the rate of evaporation. As the rate of evaporation is increased, i.e., as the chemical potential becomes more negative, the ring diameter decreases. As can be seen in the inset of the left panel in Figure 5, the diameter of the ring is very sensitive to small changes in the value of the chemical potential. This is consistent with the relation between the evaporation dynamics and the value of the chemical potential, as analyzed elsewhere.[50]

The effects of evaporation rate on the diameter of the ring were also discussed in the work of Ohara and Gelbart in the limit where evaporation is dominant.[43] They argued that the diameter of the ring increases upon an increase in the evaporation rate. Our observation is opposite and seems to contradict their conclusion. However, we would like to note that Ohara and Gelbart increased both the uniform and rim evaporation at the same time, whereas in our model, these rates are not completely correlated upon changing the chemical potential. Nevertheless, we believe that the picture emerging from our model is more realistic for experiments, where typically one controls the chemical potential and not the rates of evaporation.

The role of nanoparticle diffusivity on the size and shape of the rings is shown in Figure 6. We plot the final morphologies (only the lowest layer is shown) for different nanoparticle mobility for $\mu = -8\epsilon_l$, $T = (1/2)\epsilon_l$, and $\rho = 0.1$. The panels differ with respect to the value of N_{move}, which corresponds to different nanoparticle diffusion rates of (from top left to bottom right): 930, 2200, 3375, 4040, 4665, 5265, 6440, 9650, and 15 840, respectively, in units of evaporation rate (i.e., τ_l/τ_n).

The results obtained for the lowest and highest diffusion rates studied do not lead to the formation of closed rings. When the nanoparticles are sluggish (upper left panel of Figure 6), they cannot track the motion of the growing vapor rim and the resulting morphology shows traces of fingerling-like structure. This structure is interesting in its own right. The physical characteristics leading to the formation of this structure are further discussed below (see also Figure 7).

On the other hand, when nanoparticles diffuse rapidly, faster than the evaporation of the growing vapor rim, a ring that is formed at early times (not shown) breaks in several locations along the circumference of the rim as the system approaches its steady-state structure (lower right panel of Figure 6). This process, which is driven by surface tension, can occur when evaporation is slow compared to nanoparticle diffusion, such that nanoparticles that are pinned along the rim have a sufficiently large time to move away from the rim front and form small aggregates (see circled regions in the lower right panel) that are thermodynamically more stable.

For moderate diffusion rates, the assembly of nanoparticles leads to the formation of rings. This requires that the diffusion rate is comparable to the motion of the growing rim and puts upper and lower bounds on the diffusion rate. The lower and upper limits on the diffusion rate span only one order of magnitude. Within this range of diffusion rates, we find that the diameter of the ring does not depend in any noticeable way

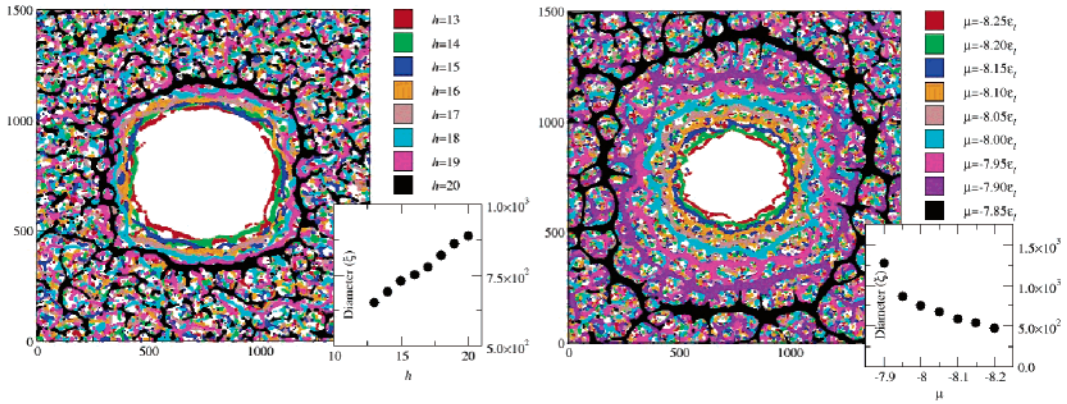

Figure 5. Plots of the final morphologies for different values of the film height (left panel) and evaporation rate (right panel). The nanoparticle coverage is $\rho = 0.1$, the temperature is $T = (1/2)\epsilon_l$, and $N_{move} = 80$ for both panels. The chemical potential is $\mu = -8\epsilon_l$ and the height of the film is $h_z = 16$ for the left and right panels, respectively. The inset shows the dependence of the ring diameter on the film height (left) and on the evaporation rate (right).

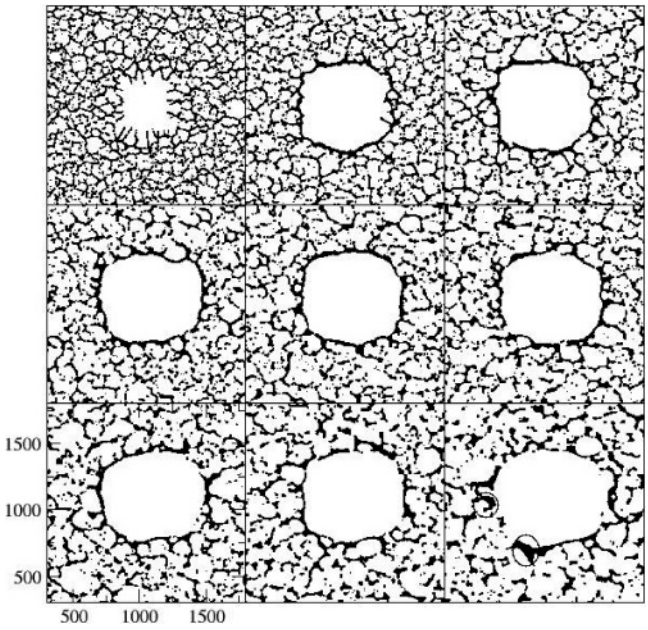

Figure 6. Final morphologies of ring formation for different nanoparticle mobility. Only the lowest layer is shown. The chemical potential, temperature, and nanoparticle density are $\mu = -8\epsilon_l$, $T = (1/2)\epsilon_l$, and $\rho = 0.1$, respectively. The value of N_{move} is (from top left to bottom right): 30, 70, 110, 130, 150, 170, 210, 310, and 510, respectively.

on the diffusion rate of the nanoparticles, as can be seen by comparing the different panels where rings are formed in Figure 6.

Returning to discuss the lower limit of diffusion rate, in Figure 7, we plot snapshots of the 3D simulated trajectory at different times at a thermodynamic state corresponding to nanoparticle coverage $\rho = 0.1$, chemical potential $\mu = -7.5\epsilon_l$, and temperature $T = (1/2)\epsilon_l$. These values of μ and T correspond to a long total evaporation time of $\tau_l \approx 1600$ MCS (400 in the case shown in Figure 2). We take a very small value of the nanoparticle mobility, i.e., $N_{move} = 5$ which corresponds to a relatively long diffusion time of $\tau_n \approx 1.2$ MCS (0.075 in the case shown in Figure 2). The values of μ, T, and N_{move} correspond to $\tau_l/\tau_n \approx 1300$, 4 times smaller than that used to generate the results shown in Figure 2. We show the positions of the nanoparticles at the even lowest eight layers (as before, $h_z = 16$).

Comparing the results shown in Figure 7 to those shown in Figure 2, we observe that the dynamics of evaporation are completely different. In both cases, the rim evaporation rate is nearly constant and differs by approximately a factor of 2. However, the uniform evaporation is completely different. For the results shown in Figure 2, the uniform evaporation rate is constant and about 20 times smaller than the corresponding rim evaporation rate. A completely different behavior for the uniform evaporation emerges for the parameters used in Figure 7. At early times, the film thickness remains almost constant. This time regime is followed by a sudden change in the film thickness as the uniform evaporation rate becomes very large. When the film thickness approaches the size of the nanoparticles, the uniform evaporation rate reduces significantly. This unique evaporation kinetics leads to the formation of the fingerling-like structures.

At early times, when the film thickness is still considerably large, nanoparticles are too sluggish to track the front of the growing vapor rim. Unlike the drying dynamics described above for other evaporation conditions, when the nanoparticles diffuse very slowly compared to the evaporation rates, self-assembly takes places at the vapor hole despite the fact the film thickness is still quite large. At later times, the vapor hole continues to grow and the nanoparticles assemble into a fingerling-like structure. The "fingers" that are "fed" from nanoparticles that are solvated in the liquid film continue to grow until the solvent evaporates completely. The length of these domains can be tuned by changing the ratio of rim evaporation rate to the uniform evaporation rate.

As far as we know, these structures have not been observed experimentally in nanoparticle assembly. However, they do resemble the structures obtained in diffusion-limited aggregation.[51]

IV. Conclusions

In this paper, we have developed a lattice gas model to study the formation of nanoparticle rings upon drying of a thin liquid layer. We focused on the case in which the driving force for hole nucleation and growth was due to evaporation. Our approach included the description of the nanoparticles as well as that of the liquid on length scales that are equal to or larger than the typical correlation length of bulk liquid.

The first set of simulations of our model was carried out to understand the microscopic mechanism of nanoparticle ring formation. We focused on the stage of hole growth, which is effectively separated from the rare event of hole nucleation in thin liquid films. We found that the basic mechanism for the formation of rings is very similar to that proposed by Ohara

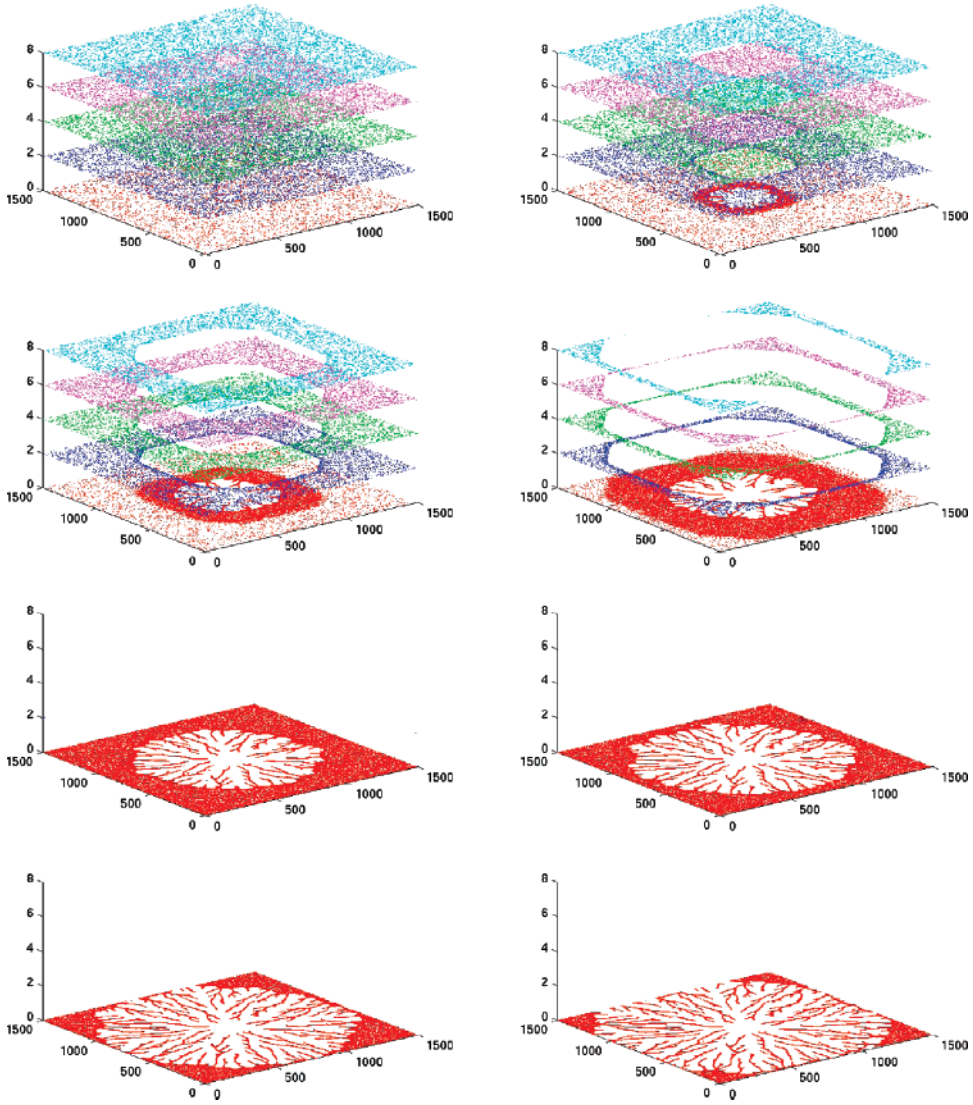

Figure 7. Snapshots of simulated trajectories at different times. From top left to bottom right: $t = 100$, 600, 1100, 1700, 2300, 2800, 3300, and 3800 in MC steps. The nanoparticle coverage, chemical potential, temperature, and nanoparticle motion are $\rho = 0.1$, $\mu = -7.5\epsilon_l$, $T = (1/2)\epsilon_l$, and $N_{move} = 5$, respectively. Different colors represent the position of nanoparticle at different layers (only the lowest eight layers are shown in steps of two layers).

and Gelbart. Namely, nanoparticles are pinned to the rim of the growing vapor hole by solvation forces. The system evolves to equilibrium by two distinct evaporation processes − one at the rim and the other is the uniform evaporation of the thin liquid film. The vapor hole continues to grow due to the former process, until the final thin liquid layer evaporates, leading to the formation of a nanoparticle ring. Furthermore, we argued that the formation of rings requires the treatment of self-assembly in 3D, because only within the 3D model can one achieve control over (a) the rate of evaporation, (b) the rate of hole growth, and (c) the rate of hole nucleation. Separate control over these properties is essential for the formation of rings.

The next set of simulations was carried out to study the role of different model parameters, such as evaporation rates, film thickness, nanoparticle density, and diffusivity on the shape and size of the resulting assembled rings. In this respect, several important conclusions can be drawn from our work. First, rings can form only if the rim evaporation rate is much larger than the uniform evaporation rate in the limit that evaporation drives the formation of rings. Furthermore, we find that the density of nanoparticles correlates (linearly) mainly with the density of nanoparticles at the ring, but not with the height or width of the ring. In addition, the diameter of the ring is very sensitive to the value of the chemical potential and somewhat less sensitive to the film thickness. Surprisingly, both the density of nanoparticles and their diffusion rates do not affect the diameter of the ring. Rings were formed only within a relatively narrow window of nanoparticle diffusion rates. When the diffusion rate is too fast, driven by surface tension, a ring that was formed at early times breaks along its circumference at latter times. When the diffusion rate is slow, fingerling-like structures, not observed experimentally, were formed. The size of the fingers can be tuned by changing the relative rates of rim evaporation and uniform evaporation.

Our coarse-grained model shares some general similarities with the approach presented by Ohara and Gelbart. However, there are also several differences. First, the mechanism by which the growth of the ring stops. We claim that the evaporation of the thin liquid layer stops the growth of the ring, whereas Ohara and Gelbart argued that it is the higher density of nanoparticles piled at the rim that leads to a high frictional force. Indeed, our model neglects frictional forces arising from the substrate, but includes collective effects that lead to self-pinning of the interface of nanoparticles. We believe that the frictional force

arising from the substrate will only slow the growth of the ring, not stop it. In some sense, our model possesses a higher frictional force induced by drying but not through increasing nanoparticle density. Ohara and Gelbart observed that for more concentrated solutions, particles accumulate more rapidly along the rim of the opening holes, leading to earlier pinning and hence smaller rings, whereas we find a negligible correlation between the size of the ring and the density of nanoparticles. Finally, we find that the faster evaporation at the rim leads to smaller rings opposite to the conclusion drawn from the work of Ohara and Gelbart. These discrepancies call for more experiments to resolve issues that are at the heart of dynamic self-assembly of nanoparticles.

Acknowledgment. We would like to thank Haim Diamant and David R. Reichman for stimulating discussions. This work was supported by the EU under the program SA-NANO (Grant STRP 013698) and by the U.S.−Israel Binational Science Foundation (Grant 2002100).

References and Notes

(1) Yin, Y.; Alivisatos, A. P. *Nature* **2005**, *437*, 664.
(2) Peng, X. G.; Manna, L.; Yang, W. D.; Wickham, J.; Scher, E.; Kadavanich, A.; Alivisatos, A. P. *Nature* **2000**, *404*, 59.
(3) Puntes, V. F.; Krishnan, K. M.; Alivisatos, A. P. *Science* **2001**, *291*, 2115.
(4) Yin, Y. D.; Rioux, R. M.; Hughes, C. K. E. S.; Somorjai, G. A.; Alivisatos, A. P. *Science* **2004**, *304*, 711.
(5) Mokari, T.; Rothenberg, E.; Popov, I.; Costi, R.; Banin, U. *Science* **2004**, *304*, 1787.
(6) Mokari, T.; Sztrum, C. G.; Shaviv, E.; Rabani, E.; Banin, U. *Nat. Mater.* **2005**, *4*, 855.
(7) Shevchenkoa, E. V.; Talapin, D. V.; O'Brien, S.; Murray, C. B. *J. Am. Chem. Soc.* **2005**, *127*, 8741.
(8) Law, M.; Goldberger, J.; Yang, P. *Annu. Rev. Mater. Sci.* **2004**, *34*, 83.
(9) Motte, L.; Billoudet, F.; Lacaze, E.; Douin, J.; Pileni, M. P. *J. Phys. Chem. B* **1997**, *101*, 138.
(10) Collier, C. P.; Vossmeyer, T.; Heath, J. R. *Annu. Rev. Phys. Chem.* **1998**, *49*, 371.
(11) Korgel, B. A.; Fullam, S.; Connolly, S.; Fitzmaurice, D. *J. Phys. Chem. B* **1998**, *102*, 8379.
(12) Sun, S.; Murray, C. B. *J. Appl. Phys.* **1999**, *85*, 4325.
(13) Murray, C. B.; Kagan, C. R.; Bawendi, M. G. *Annu. Rev. Mater. Sci.* **2000**, *30*, 545.
(14) Shipway, A. N.; Katz, E.; Willner, I. *Chem. Phys. Chem.* **2000**, *1*, 18.
(15) Huang, J.; Kim, F.; Tao, A.; Conner, S.; Yang, P. *Nat. Mater.* **2005**, *4*, 896.
(16) Tang, Z.; Kotov, N. A. *Adv. Mater.* **2005**, *17*, 951.
(17) Shevchenko, E. V.; Talapin, D. V.; Kotov, N. A.; O'Brien, S.; Murray, C. B. *Nature* **2006**, *439*, 55.
(18) Freeman, R. G.; Grabar, K. C.; Allison, K. L.; Bright, R. M.; Davis, J. A.; Guthrie, A. P.; Hommer, M. B.; Jackson, M. A.; Smith, P. C.; Walter, D. G.; Natan, M. J. *Science* **1995**, *267*, 1629.
(19) Gelbart, W. M.; Sear, R. P.; Heath, J. R.; Chaney, S. *Faraday Discuss.* **1999**, *112*, 299.
(20) Ge, G.; Brus, L. E. *J. Phys. Chem B* **2000**, *104*, 9573.
(21) Whitesides, G. M.; Grzybowski, B. *Science* **2002**, *295*, 2418.
(22) Korgel, B. A.; Fitzmaurice, D. *Phys. Rev. B* **1999**, *59*, 14191.
(23) Rabani, E.; Egorov, S. A. *J. Chem. Phys.* **2001**, *115*, 3437.
(24) Rabani, E.; Egorov, S. A. *Nano. Lett.* **2002**, *2*, 69.
(25) Rabani, E.; Egorov, S. A. *J. Phys. Chem. B* **2002**, *106*, 6771.
(26) Saunders, A. E.; Shah, P. S.; Park, E. J.; Lim, K. T.; Johnston, K. P.; Korgel, B. A. *J. Phys. Chem. B* **2004**, *108*, 15969.
(27) Lin, X. M.; Jaeger, H. M.; Sorensen, C. M.; Klabunde, K. J. *J. Phys. Chem. B* **2001**, *105*, 3353.
(28) Redl, F. X.; Cho, K. S.; Murray, C. B.; O'Brien, S. *Nature* **2003**, *423*, 968.
(29) Rabani, E.; Reichman, D. R.; Geissler, P. L.; Brus, L. E. *Nature* **2003**, *426*, 271.
(30) Stzrum, C. G.; Hod, O.; Rabani, E. *J. Phys. Chem. B* **2005**, *109*, 6741.
(31) Sztrum, C. G.; Rabani, E. *Adv. Mater* **2006**, *18*, 565.
(32) Martin, C. P.; Blunt, M. O.; Moriarty, P. *Nano Lett.* **2004**, *4*, 2389.
(33) Maillard, M.; Motte, L.; Ngo, A. T.; Pileni, M. P. *J. Phys. Chem. B* **2000**, *104*, 11871.
(34) Maillard, M.; Motte, L.; Pileni, M. P. *Adv. Mater* **2001**, *13*, 200.
(35) Stowell, C.; Korgel, B. A. *Nano Lett.* **2001**, *1*, 595.
(36) Ge, G.; Brus, L. E. *Nano. Lett.* **2001**, *1*, 219.
(37) Ohara, P. C.; Heath, J. R.; Gelbart, W. M. *Angew. Chem., Int. Ed.* **1997**, *36*, 1078.
(38) Kurrika, V.; Shafi, P. M.; Felner, I.; Mastai, Y.; Gedanken, A. *J. Phys. Chem.* **1999**, *103*, 3358.
(39) Zhou, W. L.; He, J. B.; Fang, J. Y.; Huynh, T.; Kennedy, T. J.; Stokes, K. L.; O'Connor, C. J. *J. Appl. Phys.* **2003**, *93*, 7340.
(40) Jang, J.; Oh, J. H. *Langmuir* **2004**, *20*, 8419.
(41) V., L.; Govor,; Reiter, G.; Parisi, J.; Bauer, G. H. *Phys. Rev. E* **2004**, *69*, 061609.
(42) Cheng, G. J.; Puntes, V. F.; Guo, T. *J. Colloid Interface Sci.* **2006**, *293*, 430.
(43) Ohara, P. C.; Gelbart, W. M. *Langmuir* **1998**, *14*, 3418.
(44) Elbaum, M.; Lipson, S. G. *Phys. Rev. Lett.* **1994**, *72*, 3562.
(45) TenWolde, P. R.; Sun, S. X.; Chandler, D. *Phys. Rev. E* **2001**, *65*, 011201.
(46) Chandler, D. *Introduction to Modren Statistical Mechanics*; Oxford: New York, 1987.
(47) Rabani, E.; Hetényi, B.; Berne, B. J.; Brus, L. E. *J. Chem. Phys.* **1999**, *110*, 5355.
(48) Rabani, E. *J. Chem. Phys.* **2001**, *115*, 1493. Rabani, E. *J. Chem. Phys.* **2002**, *116*, 258.
(49) Bray, A. J. *Adv. Phys.* **2002**, *51*, 481.
(50) Rabani, E.; Reichman, D. R.; Geissler, P. L.; Brus, L. E. *Nature* **2003**, *426*, 271. See on-line supplementary material.
(51) Witten, T. A.; Sander, L. M. *Phys. Rev. Lett.* **1981**, *47*, 1400.